Carcinogenesis, 2015, Vol. 36, No. 9, 1071–1083

doi:10.1093/carcin/bgv098
Advance Access publication July 7, 2015
Original Manuscript

ORIGINAL MANUSCRIPT

Artesunate induces ROS- and p38 MAPK-mediated apoptosis and counteracts tumor growth *in vivo* in embryonal rhabdomyosarcoma cells

Sara Beccafico[1,2], Giulio Morozzi[1], Maria Cristina Marchetti[3], Carlo Riccardi[3], Angelo Sidoni[1], Rosario Donato[1,2] and Guglielmo Sorci[1,2,*]

[1]Department of Experimental Medicine, University of Perugia 06132 Perugia, Italy, [2]Interuniversity Institute of Myology (IIM), Padova, Italy and [3]Department of Medicine, University of Perugia 06132 Perugia, Italy

*To whom correspondence should be addressed. Tel: +39 075 5858258; +39 075 5858415; Email: guglielmo.sorci@unipg.it

Correspondence may also be addressed to Rosario Donato. Tel: +39 075 5858256; +39 075 5858415; Email: rosario.donato@unipg.it

Abstract

Rhabdomyosarcoma represents about 50% of soft-tissue sarcomas and 10% of malignant solid tumors in childhood. Embryonal rhabdomyosarcoma (ERMS) is the most frequent subtype, suggested to have an origin in muscle precursor cells that fail to exit the cell cycle and terminally differentiate mainly because of overexpression of the transcription factor, PAX7, which sustains proliferation, migration and invasiveness in ERMS cells. Artesunate (ARS) is a semi-synthetic derivative of artemisinin (ART), a natural compound well known as an antimalarial drug. However, ART and its derivatives have been found efficacious even as anticancer drugs that induce cell cycle arrest and/or apoptosis in several kinds of cancer. Here, we show that ARS dose-dependently induces DNA damage and apoptosis in ERMS cell lines. Production of reactive oxygen species (ROS) and activation of p38 MAPK have a central role in triggering ARS-mediated apoptosis in ERMS cells; indeed either the antioxidant, N-acetylcysteine or the p38 MAPK inhibitor, SB203580, protects ERMS cells from ARS-induced apoptosis. Moreover, ARS treatment in ERMS cells ROS-dependently induces the expression of the myo-miRs, miR-133a and miR-206, which are down-regulated in RMS, and reduces PAX7 protein levels. Finally, ARS upregulates the expression of the adhesion molecules, NCAM and integrin β1, and reduces migration and invasiveness of ERMS cells *in vitro*, and ARS treatment reduces of about 50% the growth of ERMS xenografts *in vivo*. Our results are the first evidence of efficacy of ART derivatives in restraining ERMS growth *in vivo*, and suggest ARS as a potential candidate for therapeutic treatment of ERMS.

Introduction

Rhabdomyosarcoma (RMS) is the most common soft-tissue sarcoma in childhood (1,2). RMSs are divided into two main histological variants, which are associated with different frequency and prognosis: alveolar RMS (ARMS) and embryonal RMS (ERMS). ARMSs develop in older children and adolescents, and are characterized by t(2,13)(q35;q14) or t(1,13)(p36;q14) chromosomal translocations that fuse the transcription factors of paired box family, PAX3 or PAX7, respectively, to FoxO1A, a member of the fork-head transcription factor family. These events generate potent transcription factors that sustain ARMS tumor properties (3). Conversely, ERMSs are more frequent in childhood, do not present recurrent chromosomal translocations, are characterized by loss of heterozygosity and imprinting on different chromosomal loci, and typically overexpress PAX7 (3,4). PAX7 sustains proliferation, migration and invasiveness and its expression in myoblasts needs to diminish for terminal differentiation to occur (5,6). While ARMSs are believed to originate from mesenchimal cells, an origin from muscle precursor

Received: October 20, 2014; **Revised:** June 25, 2015; **Accepted:** July 1, 2015

Abbreviations

ARMS	alveolar RMS
ART	artemisinin
ARS	artesunate
DHA	dihydroartemisinin
DMEM	Dulbecco's modified Eagle's medium
ERMS	embryonal RMS
FACS	fluorescence-activated cell sorting
GM	growth medium
MAPK	mitogen-activated protein kinase
NAC	N-acetylcysteine
PBS	phosphate-buffered saline
PI	propidium iodide
RMS	rhabdomyosarcoma
ROS	reactive oxygen species

cells/differentiating myoblasts has been suggested for ERMSs (7,8). Indeed, ERMSs resemble myoblasts unable to differentiate despite the expression of markers of muscle lineage (e.g. the transcription factors, MyoD and myogenin) as well as structural proteins (e.g. myosin heavy chain, skeletal α-actin and desmin) (2,3).

Contrary to other tumors, such as Hodgkin lymphoma, retinoblastoma, Wilms tumor and germ cell tumors, for which the survival rate exceeds 90% thanks to the discovery of efficient cytotoxic chemotherapeutic agents, chemotherapy still remains largely non-effective in the treatment of RMS (9). Thus, discovery of novel drugs able to induce death of therapy-resistant tumor cells is advisable.

Artemisinin (ART) is a sesquiterpene lactone extracted from the Chinese herb, *Artemisia annua* L. (sweet wormwood) used for more than 2000 years in the treatment of several illness, and later employed in malaria treatment (10,11). More recently, ART and its derivatives were shown to exhibit potent anticancer properties in a variety of tumor types, including lung, pancreatic, ovarian, colorectal, prostate and breast cancer *in vitro* and *in vivo* (12, and references therein). The antimalarial activity of ART and its derivatives mainly resides in the endoperoxide bond present in their molecular structure. Once activated by reduced heme or ferrous iron that are abundant in *Plasmodium*, this endoperoxide bond leads to formation of cytotoxic products that cause parasite death (13,14). For this reason, the high iron levels typical of tumor cells and required for sustaining elevated cancer cell proliferation rate make tumor cells highly susceptible to the action of ART and ART derivatives, whereas their normal counterparts result less sensitive (12). Nevertheless, the specific mechanisms of the anticancer activity and primary targets of ART and ART derivatives are not fully understood. Induction of apoptosis, growth arrest, inhibition of angiogenesis and metastasis formation were reported as effects of these drugs on different kinds of tumor cells (12,15). It has been shown that dihydroartemisinin (DHA), one of the semi-synthetic ART derivatives, determines cell growth arrest and apoptosis in the RMS cell lines, Rh30 and RD by blocking mTORC1-mediated signaling pathways (16). These results prompted further studies to better understand the anticancer properties of ART derivatives in RMS, and opened perspectives for a more efficient anticancer therapy. Artesunate (ARS) was developed as a more stable and effective derivative of ART, with an excellent safety profile, largely recommended by the World Health Organization (WHO) for malaria treatment (17). Moreover, ARS has been used in combination with standard chemotherapy for the treatment of two human melanoma cases with encouraging results (18). In the present work, we report the effects of ARS treatment on ERMS cells *in vitro* and *in vivo*. We show that ARS exerts on ERMS cells a cytotoxic effect mediated by reactive oxygen species (ROS) production and p38 MAPK activation. Importantly, ARS does not show significant toxicity towards normal myoblasts, even at high doses. In ERMS cells, ARS ROS-dependently upregulates the muscle-specific microRNAs, miR-133a and miR-206, which are typically downregulated in RMSs, and reduces the protein levels of PAX7, whose activity sustains tumor behavior in ERMS cells. When treated with ARS ERMS cells upregulate the expression of NCAM and integrin β1, which translates into reduced cell migration and invasiveness *in vitro*. Finally, intraperitoneal administration of ARS alone to ERMS-bearing mice is sufficient to significantly reduce cell proliferation and tumor growth *in vivo*.

Materials and methods

Cell culture

TE671 (ATCC #CRL-8805), RD18 (Pier-Luigi Lollini, Bologna, Italy) (19) and C2C12 myoblasts were cultured in high-glucose Dulbecco's modified Eagle's medium (HG-DMEM) containing 5% (TE671 cells), 10% (RD18 cells) or 20% (C2C12 cells) fetal bovine serum, 100 U/ml penicillin and 100 U/ml streptomycin (growth medium, GM) in a humidified atmosphere of 5% CO_2 at 37°C. After receipt, cells were expanded and aliquots were frozen in liquid nitrogen; each aliquot was used for no more than 10 passages.

FACS analyses

TE671, RD18 or C2C12 cells were seeded onto 35-mm plastic dishes (2.0×10^5 cells/dish) and treated with different doses of DHA or ARS (both from Sigma–Aldrich) for 24 h in GM. Cells treated with ARS were also cultured in the absence or presence of either N-acetylcysteine (NAC) (10 mM; Sigma–Aldrich) or SB203580 (5 μM; Calbiochem), as indicated. After 24 h of treatment, the apoptotic cells suspended in the medium were collected, washed twice with phosphate-buffered saline (PBS) and resuspended in 1 ml propidium iodide (PI) solution (0.1% sodium citrate, 0.1% Triton X-100, and 50 mg/l PI) (20). The percentages of sub-G1 cells were evaluated by flow cytometry using a fluorescence-activated cell sorting (FACS, Coulter Epics XL-MLC). Annexin V labeling and PI staining was carried out in TE671, RD18 and C2C12 cells 24 h after the indicated treatment according to the manufacturer instructions (FITC Annexin V/Dead Cell Apoptosis kit; Life Technologies). Cell cycle progression was analyzed via PI staining. After 24 h of treatment with the indicated doses of ARS ERMS and C2C12 cells were washed twice with PBS and incubated 30 min in the dark at 4°C with 700 μl of PI. Cells in the different phases of cell cycle were evaluated by flow cytometry analysis. In several experiments, cells were labeled with BrdU and 7-amino-actinomycin D (7-AAD). BrdU (10 μM) was added to the cells 24 h after treatment with the indicated doses of ARS. After additional 2 h, the cells were processed as recommended by the manufacturer (FITC BrdU Flow kit; BD Pharmingen) and evaluated for the percentages of BrdU-positive cells in the S phase of the cell cycle by FACS analysis. All experiments were repeated at least three times.

ROS measurement

TE671, RD18 or C2C12 cells were plated (3.0×10^3 cells) onto 96-well plates and treated with different doses of ARS for 24 h. Growth medium was replaced with phenol-free DMEM containing 10 μM dihydrorhodamine 123 (DHR; Invitrogen). After 30 min, cells were washed twice with PBS and fluorescence was measured at 500 nm excitation and 536 nm emission wavelengths by a fluorescent reader (TECAN infinite M200). Relative ROS levels were expressed as fold increase in DHR fluorescence compared with the control.

Immunofluorescence

TE671, RD18 or C2C12 cells were plated on cover glasses and treated with different doses of ARS in the absence or presence of NAC (10 mM) for 24 h. Cells were fixed for 20 min in 3.7% paraformaldehyde in PBS, washed three times with PBS and incubated with 1% Triton X-100 for 10 min. After washes with PBS, cells were incubated in blocking buffer (3% bovine serum albumin, 1% glycine in PBS) for 1 h at room temperature (r.t.) followed by incubation with an antiphospho histone H2A.X (Ser139) monoclonal antibody (1:300; Millipore). After washes with 0.1% Tween-20 in PBS, the cells were incubated

with Alexa fluor 488 donkey anti-mouse antibody (1:200; Invitrogen) for 1 h at r.t. Nuclei were counterstained with 4′,6-diamidino-2-phenylindole (DAPI, 1 μg/ml; Sigma–Aldrich). After mounting, the cells were viewed in a DM Rb epifluorescence microscope (Leica) equipped with a digital camera.

Western blotting

See Supplementary material for details.

Real-time PCR

See Supplementary material for details.

Wound-healing assay

TE671 or RD18 cells were seeded onto six-well plates (4.0×10^5 cells/well) in GM and after 24 h, a straight scratch, simulating a wound, was made using a pipette tip. Then, the cells were cultured in the presence or absence of ARS (0.5 or 5.0 μM) for an additional 24 h. Images were taken immediately after scratching (t0) and 24 h later (t24). The migration rate was expressed as the percentage of the gap distance covered by migrating cells.

Invasiveness assay

TE671 or RD18 cells (1.0×10^5 cells) were seeded in the upper chamber of BioCoat Matrigel invasion chambers (pore size, 8 μm) (BD Biosciences) in DMEM containing 2% fetal bovine serum, and DMEM with 10% fetal bovine serum was placed in the lower chamber (21). After 20 h, the cells migrated to the lower side of the chamber were fixed in methanol, stained with crystal violet and counted under a microscope (10 randomly chosen fields per sample).

In vivo tumorigenesis assay

Five-week-old female athymic *nu/nu* mice (Harlan Laboratories) were injected subcutaneously with TE671 cells resuspended in serum-free DMEM (3.5×10^6 cells; total volume, 0.5 ml) into their right flanks. Mice were maintained in a sterile environment and received food and water ad libitum. At the appearance of tumor masses, mice were randomized into two groups: ARS-treated animals (n =10), which received a daily intraperitoneal injection with freshly prepared ARS (25 mg/kg body weight in DMEM), and mock-treated animals (n = 9), which received a daily intraperitoneal injection with vehicle (i.e. equivalent amount of dimethyl sulfoxide in DMEM). Tumor size and body weight were measured every 3 days and the tumor volumes were estimated using the formula $1/2axb^2$, where a stands for the long diameter and b for the short diameter (22). The mice were closely monitored for 15 days following tumor appearance, and the experimentation was stopped by killing of the animals. Tumors were removed and measured. Mouse bodies devoid of tumor masses were weighted. Approval of use of animals was obtained by the Ethics Committee of the University of Perugia, and animal experimentation has followed the principles of the three Rs (Replacement, Reduction, Refinement) in accordance with the Directive 2010/63/EU of the European Union.

Histology and immunohistochemistry

See Supplementary material for details.

Statistical analysis

Each *in vitro* experiment was repeated at least three times. Representative experiments are shown unless stated otherwise. Quantifications on tumor sections were performed by three independent operators blinded to treatments. Twenty randomly chosen fields (magnification, ×20) were counted for each section. Areas with sectioning artifacts (folds, tears, etc.) were avoided. Quantitative data are presented as mean ± SEM. The data were subjected to analysis of variance (ANOVA) with SNK *post hoc* analysis using a statistical software package (GraphPad Prism version 4.00, GraphPad).

Results

ARS dose-dependently induces apoptosis in ERMS cells but not in normal myoblasts

We tested increasing (0–50 μM) doses of ART, DHA or ARS on cell viability and apoptosis in the ERMS cell lines, TE671 and RD18, and in C2C12 myoblasts. ART did not significantly affect ERMS and C2C12 cell numbers after 24 h of treatment even at the highest dose used. However, DHA dose-dependently reduced TE671 and RD18 cell numbers, with the strongest effect being observed on TE671 cells (IC_{50} = 50 μM) (Supplementary Figure 1A, available at *Carcinogenesis* Online). Neither ART nor DHA significantly affected C2C12 myoblasts viability (Supplementary Figure 1A, available at *Carcinogenesis* Online), in accordance with reported data (16). ARS reduced C2C12 cell numbers only at concentrations ≥10 μM, albeit to a very low extent (Figure 1A). However, ARS was more efficient than DHA at reducing the numbers (IC_{50} = 10 μM) of TE671 and RD18 cells (compare Figures 1A and Supplementary Figure 1A, available at *Carcinogenesis* Online), which showed a similar sensitivity to the drug. Phase-contrast microscopy revealed elevated numbers of detached cells in the case of TE671 and RD18 cells, and substantially unaffected morphology of C2C12 monolayers in the presence of 25 or 50 μM ARS, although C2C12 cell numbers appeared slightly reduced (Supplementary Figure 1B, available at *Carcinogenesis* Online). After 24 h DHA or ARS dose-dependently induced cell death in TE671 and RD18 cells, with ARS being more effective than DHA (19.7 versus 8.6% and 44.0 versus 19.7% sub-G1 cells at 25 and 50 μM ARS, respectively, compared to DHA) as assessed by FACS analysis (Figure 1B and Supplementary Figure 1C and D, available at *Carcinogenesis* Online). Whereas DHA was more effective on TE671 than RD18 cells at inducing cell death, ARS showed a similar efficacy on both ERMS cell lines. Notably, the percentages of sub-G1 cells were unaffected by either DHA or ARS in normal myoblasts even at the higher doses used (Figure 1B and Supplementary Figure 1C, available at *Carcinogenesis* Online). FACS analysis of externalized phosphatidylserine revealed that ARS dose-dependently activated the apoptotic process in TE671 and RD18 cells (14.2 and 11.8% apoptotic cells, respectively, in the presence of 25 μM ARS) (Figure 1C). Consistently, at concentrations ≥10 μM ARS induced the cleavage of caspase 3 into its (proapoptotic) active fragments in ERMS cells (Figure 1D).

Cytofluorimetric analysis of the cell cycle showed a decrease in the percentage of cells in G0/G1 phase in both ERMS and C2C12 cells treated with ARS (~44 versus ~54% and 49.3 versus 58.6% for ERMS and C2C12 cells, respectively, treated with 25 μM ARS compared with control cells) (Figure 1E and Supplementary Figure 1E, available at *Carcinogenesis* Online). Also, ARS dose-dependently induced accumulation of cells in S or G2/M phase in ERMS cells and normal myoblasts, respectively. Indeed, (i) ~39% TE671 and RD18 cells were found in S phase after treatment with 25 μM ARS, whereas ~30% cells were in S phase in untreated controls; and, (ii) ~31% C2C12 myoblasts were in G2/M phase in the presence of 25 or 50 μM ARS compared with 16.3% cells in G2/M phase in untreated controls. The percentages of cells in G2/M phase were substantially unaffected by ARS in ERMS cells, as were the percentages of cells in S phase in the case of C2C12 cells. Since data pointed to a lengthening in the progression in S phase of ERMS cells, we performed analysis of BrdU uptake concurrently with flow cytometry DNA content analysis. We found a significant decrease in S phase BrdU-labelled cells after a 2-h BrdU pulse in ERMS cells previously exposed for 24 h to ARS (Figure 1F). Moreover, in these cells the mean intensity of BrdU staining appeared reduced after treatment with ARS (Figure 1F). Thus, after ARS exposure there is a higher number of cells in S phase (Figure 1E) and these cells have less propensity to incorporate BrdU, as evidenced by both the reduced number of BrdU-positive cells and the reduced BrdU incorporation rate in S phase cells (Figure 1F). This pointed to ARS-induced lengthening of S phase and consequent reduction of the proliferation rate in ERMS cells. Supporting an ARS-induced

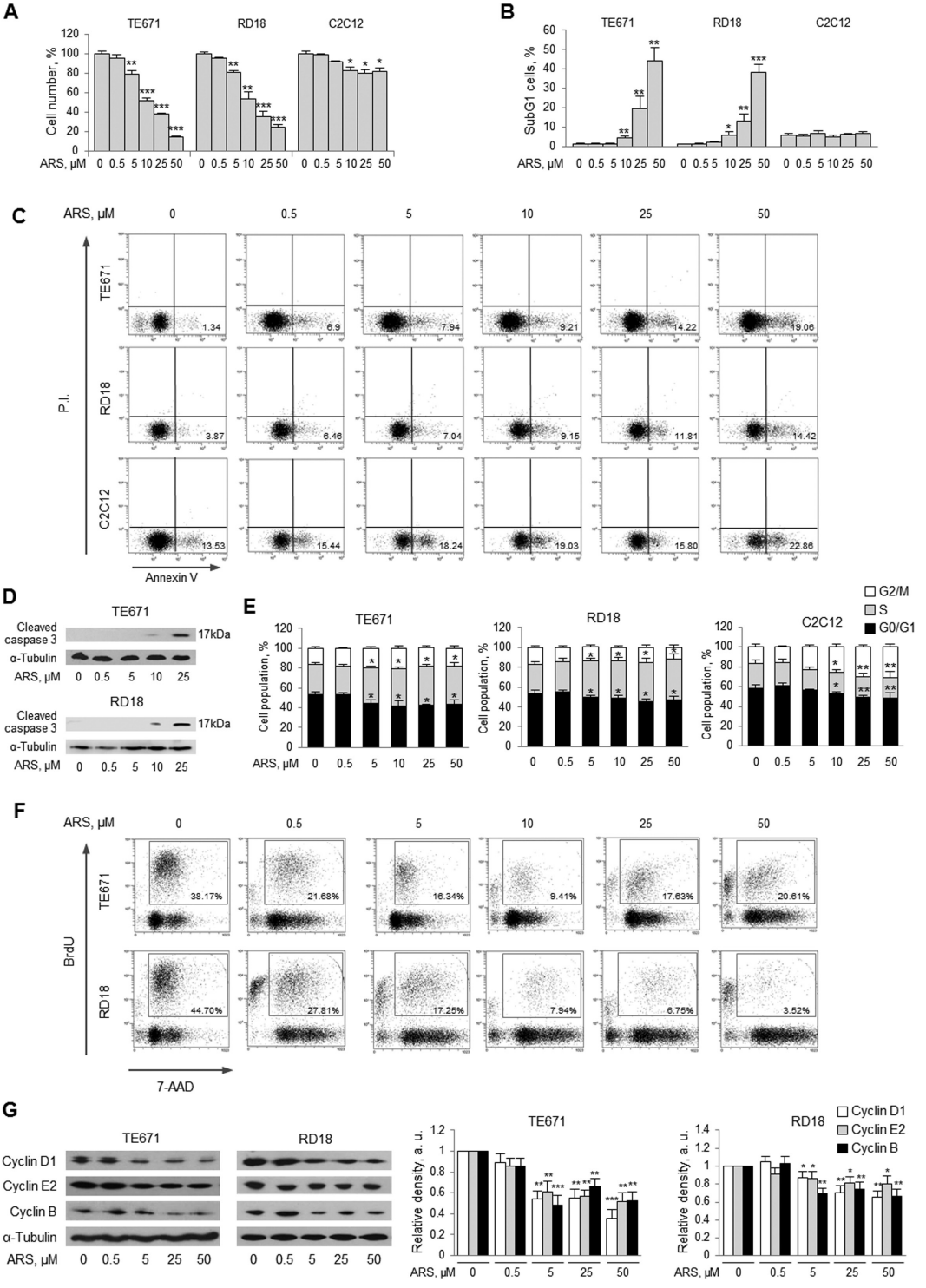

Figure 1. ARS induces apoptosis in ERMS cells but not in normal myoblasts. (**A**) Numbers of TE671, RD18 and C2C12 cells cultured in growth medium (GM) and treated with increasing doses of ARS (0–50 μM) for 24 h were calculated by cell count. Reported are the percentages of cell numbers compared with control cells. (**B**, **C**) TE671, RD18 and C2C12 cells treated as in A were analyzed for the percentages of sub-G1 (B) and apoptotic (C) cells by flow cytometry after propidium iodide (PI) and annexin V/PI staining, respectively. Representative flow cytometry dot plots with the percentages of apoptotic cells are reported (C). (**D**) Whole extracts of TE671 and RD18 cells treated with increasing (0–25 μM) doses of ARS for 24 h in GM were analyzed for cleaved (activated) caspase 3 by western blotting. (**E**) The cell cycle of TE671, RD18 and C2C12 cells treated as in A was determined by flow cytometry after PI staining. Reported are the percentages of cells in G2/M, S or G0/G1 phase in each experimental condition. (**F**) Asynchronous TE671 and RD18 cells were exposed to different doses of ARS (0–50 μM) for 24 h in GM before being labeled with BrdU. After additional 2 h, cells were collected and BrdU incorporation and 7-AAD content were quantified by FACS analysis. Cells residing inside the boxed areas were considered as residing in the S phase of the cell cycle. The percentages of S phase BrdU-positive cells in each condition are indicated. (**G**) TE671 and RD18 cells treated with the indicated doses of ARS for 24 h in GM were analyzed for the expression of cyclins D1, E2 and B by western blotting (*left panels*). Relative amounts are reported for each cyclin compared to control cells (*right panels*). α-Tubulin (D,G) was used as internal loading control. Results are the means (±SEM) of three independent experiments. *P ≤ 0.05, **P ≤ 0.01, ***P ≤ 0.001 compared with untreated control.

reduction of cell proliferation, we found that ARS dose-dependently reduced the expression of cyclins B, D1 and E2 in both TE671 and RD18 cells compared with untreated controls (Figure 1G).

ARS-induced apoptosis is a ROS-mediated event in ERMS cells

ART and ART derivatives are known to induce production of ROS in responsive cells (13,14). Thus, we analyzed the relative amounts of ROS in ERMS and C2C12 cells in the presence of increasing doses of ARS. ARS dose-dependently stimulated ROS production in TE671 and RD18, but not C2C12 cells (Figure 2A), and the antioxidant and ROS scavenger, NAC (10 mM) almost completely abolished the effect of ARS on ERMS cell viability as assessed by cell counts and phase contrast microscopy analysis (Figure 2B and Supplementary Figure 2A and B, available at *Carcinogenesis* Online). Thus, ARS-induced apoptosis was

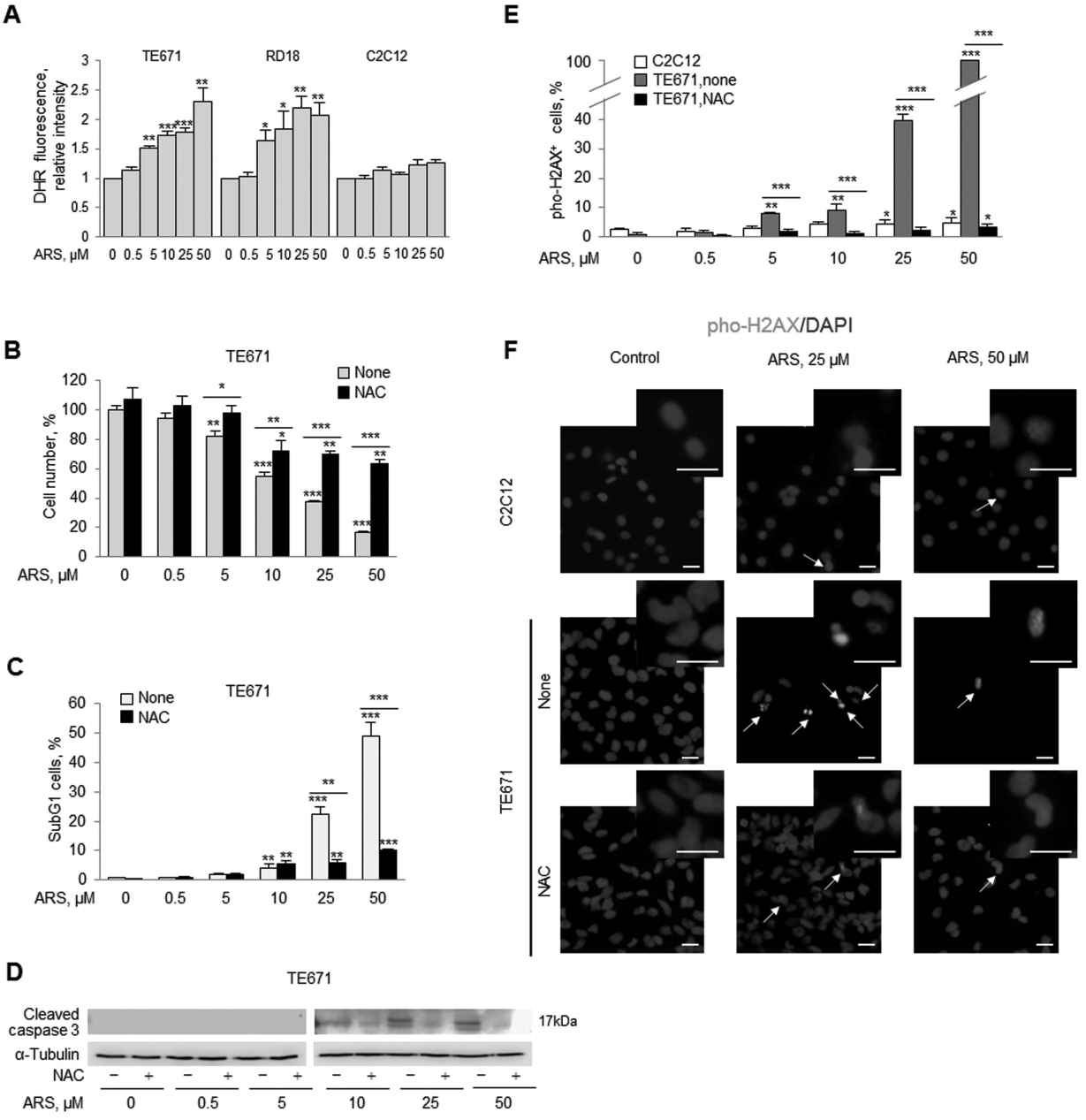

Figure 2. ARS-induced apoptosis is triggered by ROS production. (**A**) TE671, RD18 and C2C12 cells cultured in the presence of increasing (0–50 μM) doses of ARS for 24 h in GM were analyzed for ROS generation by DHR fluorescence. Reported are relative DHR fluorescence intensities compared with control cells. (**B**) TE671 cells were treated with 10 mM NAC before exposure to increasing (0–50 μM) doses of ARS for 24 h in GM. Reported are cell counts expressed as percentages versus control. (**C**) TE671 cells treated as in B were analyzed for the presence of sub-G1 cells (%) by flow cytometry after PI staining. (**D**) TE671 cells were incubated in the absence (–) or presence (+) of NAC before being exposed to increasing (0–50 μM) doses of ARS for 24 h in GM. Whole extracts were analyzed for cleaved caspase 3 by western blotting. α-Tubulin was used as internal loading control. (**E**) TE671 and C2C12 cells treated as in A, B were analyzed for phosphorylation levels of histone H2A.X (pho-H2A.X) by immunofluorescence staining. Reported are the percentages of pho-H2A.X^{+ve} cells in each experimental condition. (**F**) Representative images of C2C12 and TE671 cells treated or not treated with ARS (25 or 50 μM) following immunofluorescence staining of pho-H2A.X. TE671 cells cultured in the presence of NAC are also shown. Cells were counterstained with DAPI. Arrows point to pho-H2A.X^{+ve} cells. Insets at higher magnification are shown. Results (A–C, E) are the means (±SEM) of three independent experiments. Original magnification (F), ×20. *$P \leq 0.05$, **$P \leq 0.01$, ***$P \leq 0.001$ compared with internal control. See online Supplementary material for a colour version of this figure.

probably linked to ARS-induced ROS generation. Moreover, NAC treatment translated into a dramatic reduction of ARS-induced cell death (sub-G1 cells) in ERMS cells (73.2 and 79.6% reduction in the presence of 25 and 50 μM ARS, respectively, in the case of TE671 cells) (Figure 2C and Supplementary Figure 2C, available at *Carcinogenesis* Online). Accordingly, ARS-induced cleavage of caspase 3 was robustly reduced by pretreatment with NAC in both TE671 and RD18 cells (Figure 2D and Supplementary Figure 2D, available at *Carcinogenesis* Online). Histone H2A.X is rapidly phosphorylated following double-stranded DNA breaks, and is required for DNA fragmentation during apoptosis (23). We found increasing phosphorylation of H2A.X in ERMS cells, but not C2C12 cells, after incubation with increasing doses of ARS. Pretreatment with NAC almost completely abrogated the ability of ARS to induce DNA damage in ERMS cells (Figure 2E and F and Supplementary Figure 2E and F, available at *Carcinogenesis* Online). These results pointed to a major role of ROS in ARS-induced ERMS cell death.

p38 MAPK is involved in ARS-induced apoptosis in ERMS cells

We analyzed the activation level of several kinases involved in cell survival and/or apoptosis, and of the transcription factor, NF-κB, in ERMS and C2C12 cells in the presence of increasing (0–50 μM) doses of ARS. ARS treatment in ERMS cells dose-dependently caused an increase in the phosphorylation levels of ERK1/2 and p38 MAPK, a significant decrease in phosphorylation levels of the pro-survival kinase, Akt, and a dramatic decrease in the active form of canonical NF-κB, p65 (Figure 3A and Supplementary Figure 3A, available at *Carcinogenesis* Online). No significant changes in phosphorylation levels of p65 and the kinases above could be documented in ARS-treated C2C12 myoblasts (Figure 3A). When ERMS cells were cultured in the presence of NAC, effects of ARS on p38 MAPK and p65 phosphorylation levels were partly abrogated, and Akt phosphorylation was increased (Figure 3B and Supplementary Figure 3B, available at *Carcinogenesis* Online). Thus, ARS effects on ERMS cells were dependent on ROS generation in part. Contrariwise, ARS-induced phosphorylation of ERK1/2 was further increased or nearly unaffected by pre-treatment with NAC in the case of TE671 and RD18 cells, respectively (Figure 3B and Supplementary Figure 3B, available at *Carcinogenesis* Online), pointing to a stress-induced, pro-survival role of these kinases in our experimental conditions. p38 MAPK has a key role in the differentiation process of muscle precursor cells, and its activation (phosphorylation) is associated with increased apoptosis through phosphorylation of H2A.X (24). Inhibition of p38 MAPK activity using the chemical inhibitor, SB203580, translated into increased cell numbers and reduced apoptosis in ARS-treated ERMS cells (Figure 3C and D and Supplementary Figure 3C and D, available at *Carcinogenesis* Online). Altogether, these data suggested a role for p38 MAPK in the ARS-induced apoptosis in ERMS cells. Interestingly, ARS also inhibited the phosphorylation of mTOR (S2448) and the mTORC1 downstream effector, 4E-BP1 (Supplementary Figure 3E, available at *Carcinogenesis* Online), suggesting that ARS exerts its effects in part by inhibiting mTORC1 signaling, as reported for DHA (16).

ARS induces ROS-dependent, p38-independent expression of the myo-miRs, miR-133a and miR-206, in ERMS cells

Myo-miRs are muscle-specific microRNAs strictly related to myogenic transcription factors, and involved in fundamental processes of myogenesis including myoblast proliferation, migration and differentiation (25–27). Among myo-miRs, miR-133a and miR-206 promote the differentiation of muscle precursor cells (28) and are downregulated in RMS (29). ARS dose-dependently upregulated the expression of miR-133a and miR-206 in ERMS cells (3.6 and 4.4-fold increase for miR-133a and miR-206, respectively, at the lowest dose of ARS used in the case of TE671 cells) (Figure 4A and Supplementary Figure 4A, available at *Carcinogenesis* Online). Pre-treatment of ERMS cells with NAC, but not SB203580 significantly hampered the ability of ARS to increase miR-133a and miR-206 levels (Figure 4B and C and Supplementary Figure 4B and C, available at *Carcinogenesis* Online), suggesting a role for ROS but independence from p38 MAPK in the induction of these myo-miRs under the experimental conditions used.

MiR-206 represses the translation of *PAX7* (30), a transcription factor characteristically overexpressed in ERMS cells and involved in their unrestricted proliferation and defective differentiation (3,4). Treatment of ERMS cells with ARS caused a dose-dependent increase in *PAX7* mRNA and a simultaneous reduction of PAX7 protein levels (Figure 4D and E and Supplementary figure 4D and E, available at *Carcinogenesis* Online). This result could be explained by the repression exerted by miR-206 on *PAX7* mRNA (30). When ERMS cells were exposed to ARS in the presence of NAC only a modest, not significant increase in *PAX7* levels could be observed (Figure 4F and Supplementary Figure 4F, available at *Carcinogenesis* Online). However, ARS dose-dependently reduced PAX7 protein levels irrespective of the absence or presence of NAC, compared with control cells (Figure 4H and Supplementary Figure 4H, available at *Carcinogenesis* Online), likely due to the persistence of relatively high levels of its repressor, miR-206 (see Figure 4B and Supplementary Figure 4B, available at *Carcinogenesis* Online). As expected, pretreatment with SB203580, which does not affect miR-206 levels (Figure 4C), did not result in significant changes in PAX7 mRNA and protein levels in ARS-treated compared with control ERMS cells (Figure 4G andI and Supplementary figure 4G and I, available at *Carcinogenesis* Online).

Further, we investigated the expression levels of myogenin, a marker of myogenic terminal differentiation whose expression can stimulate or inhibit PAX7 expression in ERMS cells depending on its concentration (6,31,32). ARS treatment resulted in dose-dependent decrease in myogenin mRNA (*MYOG*) and protein levels (Figure 4D and E and Supplementary Figure 4D and E, available at *Carcinogenesis* Online). The expression of MyoD, an early marker of myogenic differentiation was also reduced by ARS treatment in ERMS cells (Supplementary Figure 5, available at *Carcinogenesis* Online). Pretreatment with NAC or SB203580 resulted in reduced levels of myogenin mRNA and protein compared with control cells (Figure 4F–I and Supplementary Figure 4F–I, available at *Carcinogenesis* Online), suggesting that myogenin expression is sustained by both ROS and p38 MAPK, as known. A reciprocal, proteasome-dependent inhibition between PAX7 and myogenin has been reported in normal myoblasts and ERMS cells (6,32). Thus, we performed experiments in the presence of the proteasome inhibitor, MG132, and found that MG132 induced accumulation of PAX7 and myogenin in all conditions used (Figure 4J and Supplementary Figure 4J, available at *Carcinogenesis* Online). However, ARS was able to reduce the levels of both PAX7 and myogenin also in the presence of MG132, in accordance with a transcriptional and translational control of myogenin and PAX7 expression.

Lastly, we treated with ARS TE671 cells in which myogenin had been knocked-down. We found that PAX7 mRNA and protein were unaffected by myogenin levels either in the absence

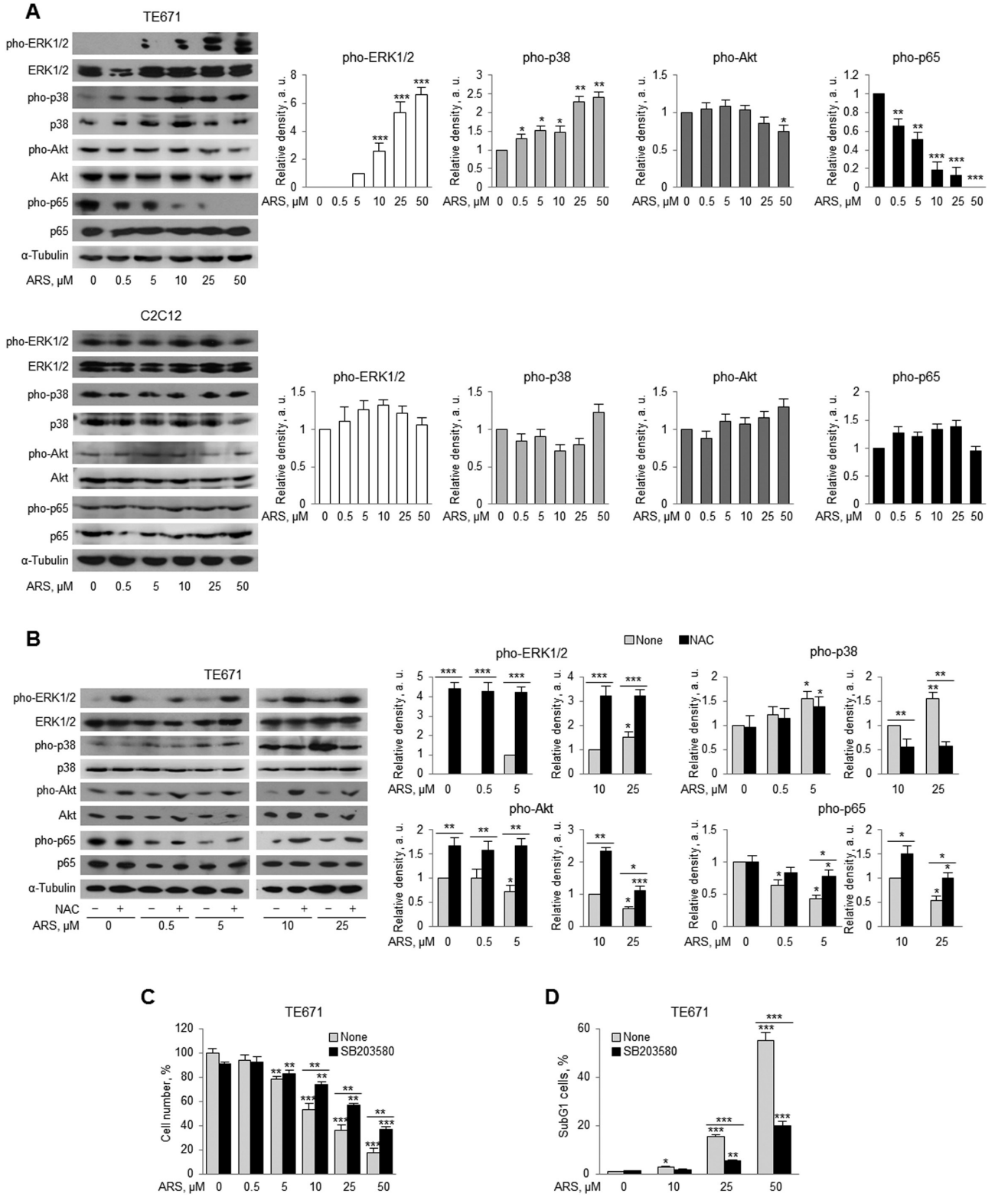

Figure 3. ARS-induced apoptosis in ERMS cells is mediated by p38 MAPK. (**A**) TE671 cells (*upper panels*) and C2C12 myoblasts (*lower panels*) treated with the indicated doses of ARS for 24 h in GM were analyzed for phosphorylation levels of ERK1/2, p38 MAPK, Akt, and NF-κB (p65) by western blotting (*left panels*). Reported are the relative densities of each factor in each condition compared with control cells (*right panels*). (**B**) TE671 cells were incubated in the absence (–) or presence (+) of NAC (10 mM) before treatment for 24 h in GM with increasing (0–25 μM) doses of ARS and subjected to western blotting for the analysis of phosphorylation levels of the factors indicated in A (*left panels*). Reported are the relative densities of each factor compared with control cells (*right panels*). (**C**) Reported are the percentages of numbers of TE671 cells after 24 h culture in GM with ARS (0–50 μM) in the absence or presence of SB203580 (10 μM). (**D**) The percentages of sub-G1 TE671 cells cultured as in C was determined by flow cytometry after PI staining. α-Tubulin (A, B) was used as internal loading control. Results are the means (±SEM) of three independent experiments. $^{*}P \leq 0.05$, $^{**}P \leq 0.01$, $^{***}P \leq 0.001$ compared with internal control.

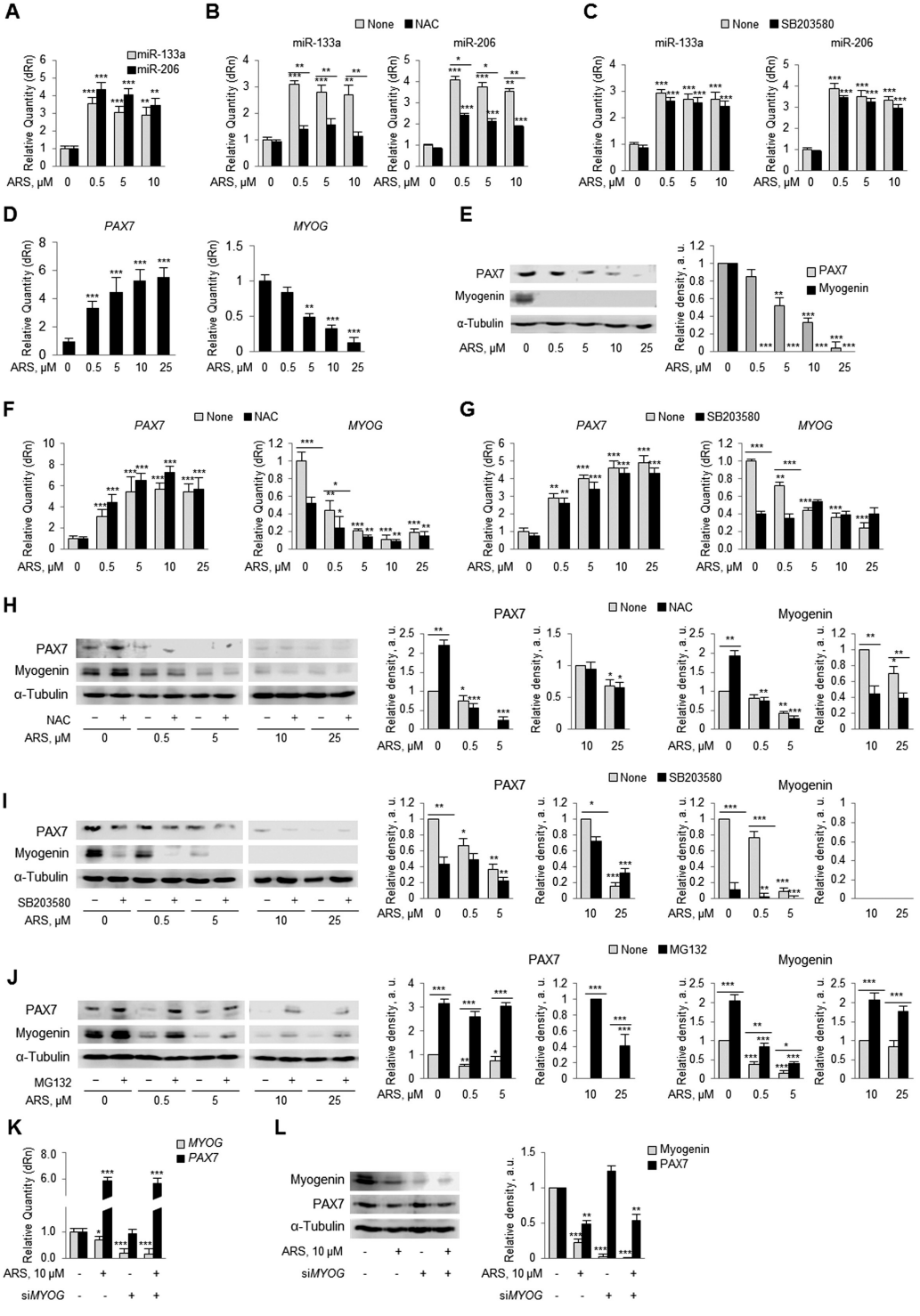

Figure 4. ARS induces upregulation of miR-133a and miR-206 in TE671 cells. (**A**) TE671 cells were cultured in the presence of the indicated doses of ARS for 24 h in GM, and expression levels of miR-133a and miR-206 were analyzed by real-time PCR. (**B**, **C**) TE671 cells treated as in A were pretreated with NAC (10 mM) (B) or SB203580 (10 μM) (C) prior to the analysis of expression levels of miR-133a (*left panels*) and miR-206 (*right panels*) by real-time PCR. (**D**) Levels of *PAX7* and myogenin (*MYOG*) mRNA in TE671 cells cultured in the presence of the indicated doses of ARS for 24 h in GM were analyzed by real-time PCR. (**E**) PAX7 and myogenin protein levels in TE671 cells treated as in D were analyzed by western blotting (*left panel*). Reported are the relative amounts with respect to control cells (*right panel*). (**F**, **G**) Levels of *PAX7* and *MYOG* mRNA in TE671 cells exposed to the indicated doses of ARS in the absence or presence of NAC (F) or SB203580 (G) were analyzed by real-time PCR. (**H**, **I**) PAX7 and myogenin protein levels in TE671 cells treated in the absence or presence of NAC (H) or SB203580 (I) as in F, G were analyzed by western blotting (*left panels*). Reported are the relative amounts with respect to control cells (*right panels*). (**J**) PAX7 and myogenin protein levels in TE671 cells cultured as in D pretreated or not with the proteasome inhibitor, MG132 (25 μM), were analyzed by western blotting (*left panel*). Reported are the relative amounts with respect to control cells (*right panels*). (**K**, **L**) TE671 cells were knocked-down for myogenin (*siMYOG*+) or treated with scramble oligonucleotides (*siMYOG*-) before being cultured for 24 h in GM in the absence or presence ARS (10 μM). Levels of PAX7 and myogenin mRNA (K) and protein (L) levels were analyzed by real-time PCR and western blotting, respectively. Reported are the relative amounts of PAX7 and myogenin proteins with respect to control cells (L; *right panel*). Results are the means (±SEM) of at least three independent experiments. α-Tubulin was used as internal loading control (E, H–J, L). *P ≤ 0.05, **P ≤ 0.01, ***P ≤ 0.001 compared with internal control.

or presence of ARS (Figure 4K and L), thus confirming the independence from myogenin of the effects of ARS on PAX7 levels in ERMS cells. Altogether, these results suggested a control by ARS on myogenin and PAX7 expression at transcriptional and translational level, and linked ARS-dependent reduction of PAX7 expression to ARS-dependent increase in miR-206 expression.

ARS reduces migration and invasiveness of ERMS cells *in vitro*

To investigate effects of ARS on migratory properties of ERMS cells, we performed classical wound healing assays *in vitro* with TE671 or RD18 cells in the presence of up to 5 μM ARS since higher concentrations of the drug were toxic to these cell lines (see Figure 1B–D and Supplementary Figure 1C, available at *Carcinogenesis* Online). TE671 and RD18 cells treated with ARS showed reduced migration rates (52.5 and 46.3% reduction, respectively, after 24 h in the presence of 5 μM ARS) (Figure 5A and Supplementary Figure 6A). Moreover, ARS caused a reduction of ERMS cell invasiveness *in vitro* even at the lowest dose used (0.5 μM) (~30 and ~15% reduction of invasiveness for TE671 and RD18 cells, respectively, compared with vehicle-treated cells) (Figure 5B and Supplementary Figure 6B, available at *Carcinogenesis* Online). Reduction of migration and invasiveness in ERMS cells was accompanied by ARS-dependent increase in the expression of the cell adhesion molecules, NCAM and integrin β1, with maximum increase after 48 h of treatment (5.7- and 3.5-fold increase for NCAM and integrin β1, respectively, in TE671 cells compared with control cells) (Figure 5C and Supplementary Figure 6C, available at *Carcinogenesis* Online).

ARS administration alone is sufficient to reduce the growth of ERMS xenografts *in vivo*

We injected subcutaneously TE671 cells (3.5×10^6 cells) into athymic *nu/nu* mice which were then treated with daily intraperitoneal injections of freshly prepared ARS (25 mg/kg body weight) or an equivalent volume of vehicle (dimethyl sulfoxide in DMEM) beginning at the appearance of the tumor mass and during the next 15 days. Measures of tumor diameters were taken every 3 days for each mouse. No significant differences could be registered between ARS- and mock-treated mice in the first few days of the experimentation. However, treatment with ARS resulted in a significantly reduced tumor growth (volume) beginning at day 6 and culminating at day 15 with about a 50% reduction of the tumor masses compared with control mice

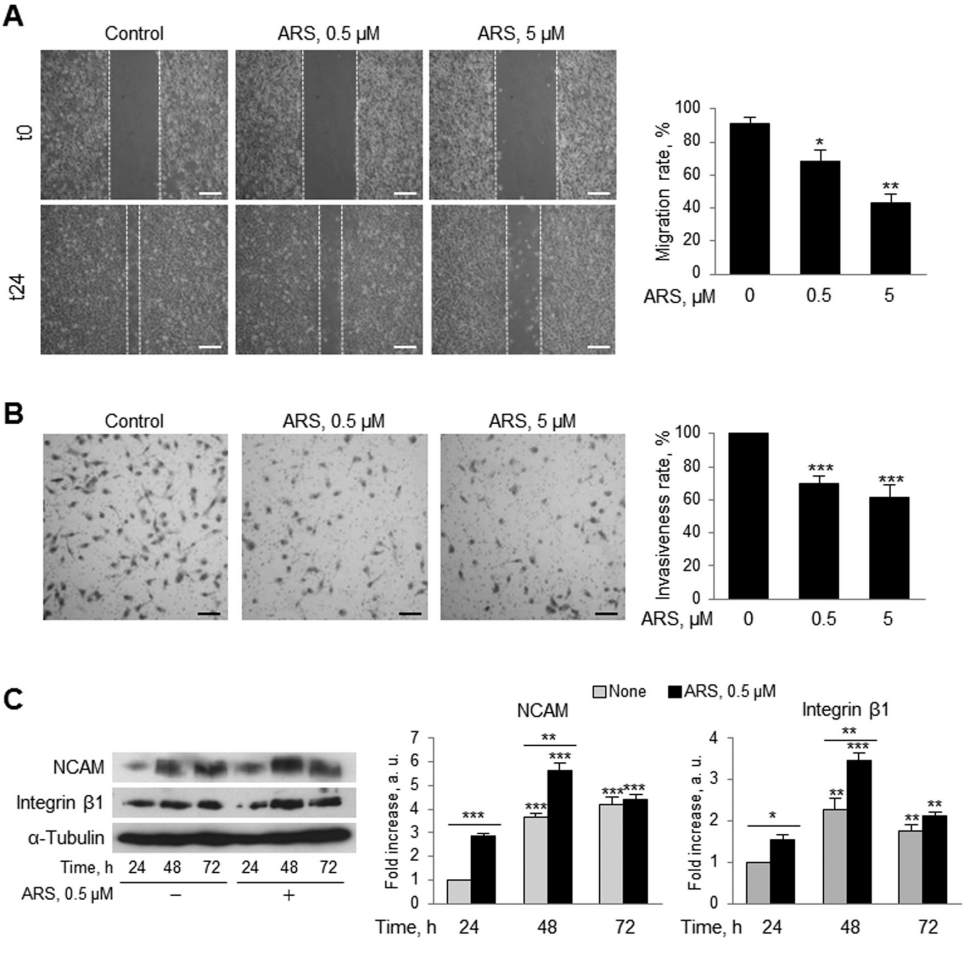

Figure 5. ARS reduces migration and invasiveness in ERMS cells *in vitro*. (**A**) Representative images of 24-h wound healing assays of TE671 cells cultured in the absence or presence of ARS (0.5 or 5 μM) were taken at the time of wounding (*t0*) and 24 h later (t24) (*left panel*). Dotted lines mark the edges of cells on the two sides of wounding. Reported is the mean percent migration 24 h after scratching (*right panel*). (**B**) The extent of invasiveness of TE671 cells treated or not treated with the indicated doses of ARS for 24 h was analyzed using Matrigel-coated cell culture inserts. Reported are representative images after fixation with methanol and crystal violet staining (*left panel*) and percentages of migrated cells in ARS-treated compared with control cells (*right panel*). (**C**) Western blotting (*left panel*) and densitometry analysis (*right panels*) of NCAM and integrin β1 in TE671 cells treated (+) or not treated (–) with 0.5 μM ARS for 24, 48 or 72 h. α-Tubulin was used as internal loading control. Original magnification (A), ×10; (B), ×20. Results are the means (±SEM) of three independent experiments. *P ≤ 0.05, **P ≤ 0.01, ***P ≤ 0.001 compared with internal control.

(Figure 6A). The mean body weight of animals after excision of the tumor mass was approximately the same in ARS- and mock-treated mice (Figure 6B), suggesting that ARS treatment does not affect body weight. Tumor masses from mice treated with ARS showed no differences in the percentage of proliferating ($Ki67^{+ve}$) cells, but a significant reduction of the percentage of cells in the mitotic phase ($H3r^{+ve}$ cells) compared with control mice (42.8 ± 7.5% versus 61.5 ± 7.1% mitotic cells in ARS- and mock-treated animals, respectively) (Figure 6C and D). Since Ki67 marks cells in all active phases of the cell cycle (i.e. G1, S, G2/M), the reduced amount of mitotic cells might reflect the lengthening of S phase as observed *in vitro* (see Figure 1E and F). In line with the results obtained *in vitro*, immunohistochemical analysis showed that tumor masses from ARS-treated mice expressed higher levels of pho-p38 and lower levels of myogenin and PAX7 (Figure 6C and E).

Discussion

RMS cells are characterized by high proliferation rate despite the expression of markers of muscle differentiation, including MyoD and myogenin. In most cases, this is due to the expression of gene-fusion transcription factors (namely, PAX3- and PAX7-FoxO1A) or high PAX7 levels in ARMS and ERMS, respectively (2–4). Moreover, RMS cells develop mechanisms to escape apoptosis, which greatly obstacles the efficacy of therapeutic interventions, so that discovery of novel anti-RMS drugs would be advisable (33).

ART is a natural compound long known for its antipyretic properties and, since 1971 for its antimalarial activity (10,11). ART and its derivatives (which include DHA, ARS and artemether) have recently emerged as powerful anticancer drugs, with minor or no effects on normal cells. This is because, contrary to their normal counterpart, malignant cells accumulate cytoplasmic iron that is important for sustaining their proliferation. Iron is an activator of ARTs reacting with their endoperoxide bonds to generate carbon-centered radicals that may mediate generation of ROS (13,14). Depending on the specific compound used, a broad range of effects have been reported in several kinds of tumor, including osteosarcoma, hepatoma, leukemia and lung and ovarian cancers in the presence of ART and/or ART derivatives, especially DHA (12,15). Recently, DHA was reported to inhibit cell proliferation and viability, and to induce apoptosis in RMS cell lines by blocking mTORC1-mediated signaling pathways (16). We obtained similar results using DHA on ERMS cells in terms of extent of proliferation and apoptosis (see Supplementary Figure 1A and C, available at *Carcinogenesis* Online). However, in the present report we focused on ARS because ARS was more efficacious than DHA at inducing cell death in ERMS cells (compare Figure 1A and B with Supplementary Figure 1A and C, available at *Carcinogenesis* Online), is known for its excellent tolerability, has been employed with promising results in two cases of uveal melanoma (18), and is under evaluation in several phase I clinical trials.

We show that treatment of ERMS cells with ARS induces apoptosis and reduces migration and invasiveness *in vitro* in a dose-dependent manner, and significantly reduces tumor growth *in vivo*. The pro-apoptotic effect is triggered by ARS-dependent induction of ROS accumulation, which becomes significant at ARS concentrations greater than 5 μM. ROS production is a common event in the treatment with ART and ART derivatives of many kinds of tumor for the reasons explained above. ROS accumulation, in turn, translates into a plethora of intracellular damages that usually culminate in caspase activation and apoptosis (34). We found ARS- and ROS-dependent appearance of double-strand breaks in the DNA, evidenced by the progressive phosphorylation of the histone H2A.X (Figure 2F and Supplementary Figure 2F, available at *Carcinogenesis* Online). In the same conditions, after exposure of ERMS cells to ARS we found unaltered percentages of cells in G2/M phase and increased percentages of cells in the S phase of the cell cycle (Figure 1E). This may indicate a defective G2/M DNA damage checkpoint in these cells, and lengthening of S phase probably reflecting the need of cells for adequate time for repairing DNA damage (35,36). ARS-induced lengthening of S phase was confirmed by BrdU incorporation analysis (Figure 1F). On the side of normal myoblasts, the reduction of C2C12 cell numbers observed in the presence of ARS (Figure 1A) seems to be due to a slower proliferation rate rather than to apoptosis, as suggested by FACS analysis (Figure 1B and C). The accumulation of C2C12 cells in G2/M phase under in the presence of the highest ARS concentrations used (Figure 1E) might reflect a cytostatic effect exerted by ARS on normal myoblasts during this specific phase of the cell cycle.

Among the observed effects of ARS on ERMS cells are a dose-dependent phosphorylation of p38 MAPK and ERK1/2, and reduced phosphorylation of the prosurvival kinase, Akt, and the transcription factor, NF-κB (p65). Pre-treatment of ERMS cells with the antioxidant, NAC, which prevents cell death in our experimental conditions (Figure 2B–D and Supplementary Figure 2A–D, available at *Carcinogenesis* Online), while decreasing p38 MAPK phosphorylation levels, increases ERK1/2 phosphorylation levels above the levels detected in control cells, and abrogates ARS-dependent reduction of Akt and p65 phosphorylation levels (Figure 3B and Supplementary Figure 3B, available at *Carcinogenesis* Online). These results suggest that ROS-induced phosphorylation of p38 MAPK has a major role in the antitumor effect of ARS in ERMS cells. Indeed, use of the p38 MAPK inhibitor, SB203580 results in a significant reduction of cell death in ERMS cells (Figure 3C,D and Supplementary Figure 3C and D, available at *Carcinogenesis* Online). Interestingly, a link exists between p38 MAPK, histone H2A.X and apoptosis, since H2A.X can be phosphorylated *in vitro* by and colocalizes *in vivo* with p38 MAPK under proapoptotic conditions (24). The reduced ability of p38 MAPK to become activated in RMS cells is long known, and forced activation of p38 MAPK leads to growth arrest and terminal differentiation in RMS cells (37). Nevertheless, p38 MAPK can be activated by stress or cytokines in RMS cells, but in these cases it fails to induce myogenic differentiation. This seems to be our case, since in ERMS cells treated with ARS we found increased phosphorylation (activation) levels of p38 MAPK with concomitant reduction of myogenin expression (Figure 4D and E). The reason why the activation of the same kinase (i.e. p38 MAPK) by different signals leads to different outcomes is an interesting matter of study. The concomitant activation or deactivation of multiple intracellular pathways actually determines the fate of a cell. In this regards, we found that ARS also inhibits mTORC1 signaling in ERMS cells (Supplementary Figure 3E, available at *Carcinogenesis* Online) as reported for DHA (16), underlying a multiple way of action of ARS in ERMSs.

By downregulating selective mRNA targets, microRNAs exert an important role in many cellular processes. We found that miR-133a and miR-206, two myo-miRs involved in myogenic differentiation (25–27) and downregulated in RMS cells (38,39), are upregulated by ARS treatment in TE671 and RD18 cells, even at the lowest dose used. Although some authors reported a stimulatory effect of miR-133 on myoblast proliferation (40), a prevalently stimulatory effect of myogenic differentiation has been attributed to this miRNA (28,41), and mRNA targets of miR-133a

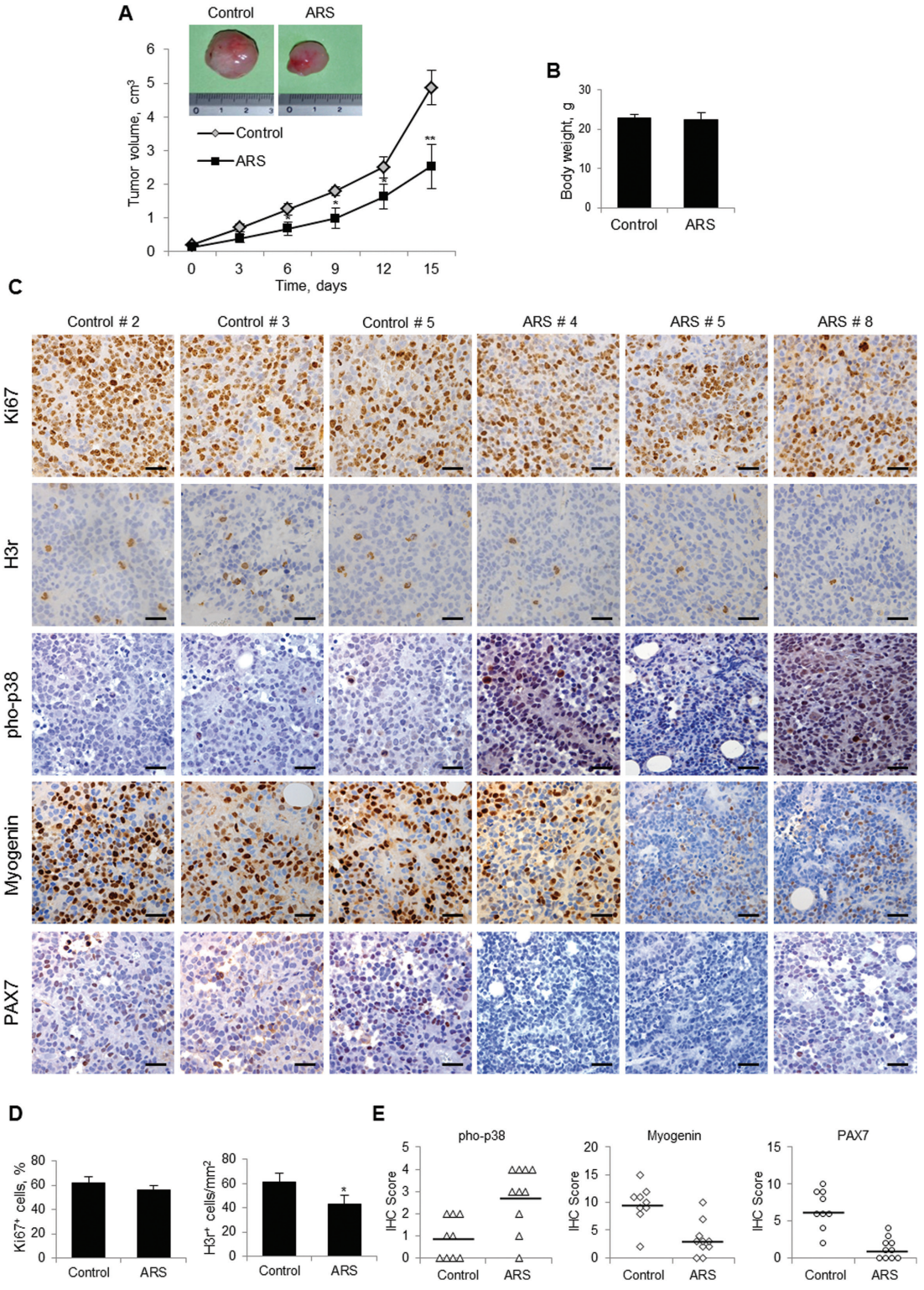

Figure 6. ARS reduces growth of ERMS xenografts *in vivo*. (**A**) Athymic *nu/nu* mice were injected subcutaneously with TE671 cells (3.5×10^6 cells/mouse). At the appearance of tumor mass, mice were daily i.p. injected with freshly-prepared ARS (25 mg/kg body weight) ($n = 10$) or vehicle ($n = 9$). Tumor diameters were measured every 3 days until day 15 and the correspondent volumes were calculated. Representative images of the tumor masses excised from control and ARS-treated mice at day 15 are reported on top of the graph. (**B**) Reported are body weights of control and ARS-treated xenograft-bearing mice in A at the end of the experimentation (i.e. 15 days after the appearance of tumor mass). (**C**) Immunohistochemical analysis of the expression of Ki67, H3r, pho-p38, myogenin and PAX7 in the tumor masses excised from control and ARS-treated mice in A. Reported are representative images of tumor masses of control (*left panels*) and ARS-treated (*right panels*) mice. (**D**) The mean percentages of $Ki67^{+ve}$ cells and the density (cells/mm^3) of $H3r^{+ve}$ cells in control and ARS-treated group in C were evaluated. (**E**) Levels of pho-p38, myogenin and PAX7 in tumor masses of control and ARS-treated mice in A were determined by attributing a score to each of them on the basis of the numbers of positive cells/field and the intensity of the immune reaction (see Materials and Methods). Original magnification (C), ×20. Results (A, B, D) are the means (±SEM). $^*P \leq 0.05$, $^{**}P \leq 0.01$ compared with untreated control.

are upregulated in RMSs (42). Moreover, ectopic expression of miR-133 inhibited cell proliferation, migration and invasion in prostate cancer cell lines (43) suggesting that miR-133 might have a role in the modulation of migration of various cell types. MiR-206 has a well-established role in myoblast differentiation (25–27), and re-expression of miR-206 in RMS cells promotes myogenic differentiation and blocks tumor growth *in vivo* (44,45). p38 MAPK signaling is required for miR-1/133a clusters transcription (41). However, in our conditions the expressions of miR-133a and miR-206 have a ROS-dependent but p38 MAPK-independent regulation. Although an increase in *MYOG* mRNA was expected in ARS-treated ERMS cells as a consequence of upregulation of miR-206, we found a dose-dependent repression of *MYOG* that was independent by both ROS and p38 MAPK after exposure to ARS.

PAX7 is a transcription factor that sustains proliferation, migration and invasiveness, and counteract myogenic differentiation in muscle precursor and ERMS cells (5,6,32). During the myogenic process miR-206 reduces PAX7 expression thus favoring cell proliferation arrest (30). This seems to be also our case since treatment with ARS leads to increased amounts of *PAX7* mRNA together with significantly reduced PAX7 protein levels. This reduction is not related to a molecular interaction between myogenin and PAX7 with subsequent reciprocal degradation through a proteasome-mediated mechanism (6,31,32) as suggested by the experiments in the presence of MG132. While we do not know the molecular mechanism underpinning ARS-induced myogenin transcriptional downregulation, our results suggest that PAX7 protein levels are mainly controlled at the translational level by miR-206.

Within the 0.5–5 μM range, i.e. at concentrations that do not significantly alter cell viability, ARS dose-dependently hampers ERMS cell migration and invasiveness *in vitro*. This is accompanied by ARS-dependent upregulation of the cell adhesion molecules, NCAM and integrin β1, and represents a potentially additional advantage in the perspective of using this drug in ERMS treatment. These results are of particular interest in consideration that the presence of metastasis is associated with a poorer prognosis in RMS patients (46,47). Recently, we reported that PAX7 downregulates *NCAM1* expression in ERMS cells thus resulting in a predominance of polysialylated (PSA)-NCAM (6), which modulates the adhesive functions of NCAM and enhances the metastatic potential of tumor cells (48). Consistently, following ARS treatment we found increased NCAM levels in experimental conditions where PAX7 protein levels were strongly diminished (compare Figure 4E and Supplementary Figure 4E, available at *Carcinogenesis* Online with Figure 5C and Supplementary Figure 6C, available at *Carcinogenesis* Online). Thus, the ARS-induced reduction in ERMS cell migration and invasiveness rate might be linked, at least in part, to downregulation of PAX7. Indeed, reduction of PAX7 levels is sufficient to reduce the tumor behavior in ERMS cells (6).

Finally, we show that ARS reduces the growth of ERMS xenografts *in vivo*. ARS treatment of ERMS-bearing mice, while counteracting tumor growth does not affect animal body weight, in line with the notion that ARS is a very well-tolerated drug (18). Immunohistochemical analysis of tumor masses revealed similar percentages of proliferating ($Ki67^{+ve}$) cells and reduced percentages of mitotic ($H3r^{+ve}$) cells in ARS - compared with mock-treated animals. This is in accordance with the results obtained by FACS analysis showing that ARS-treated ERMS cells are characterized by a lengthening of S phase, which might reduce the number of cells undergoing mitotic division. Interestingly, tumor masses from ARS-treated mice show increased phosphorylation of p38 MAPK, and reduced expression of myogenin and PAX7, as found in ERMS cells treated with ARS *in vitro*, suggesting that similar molecular events occur *in vitro* and *in vivo* in ERMS cells after exposure to ARS. To our knowledge, this is the first report of treatment of ERMS with ART derivatives *in vivo*.

Thanks to their high tolerability, ART derivatives are currently under investigation for use as anticancer drugs in humans. Data obtained so far show that different kinds of tumor respond differently to different ART derivatives (12,15), so that specific investigation is needed in view of potential use of these drugs in therapeutic protocols. Our results add novel information about the efficacy and the mechanism of action of ARS in ERMS cells. Although ARS is metabolized to DHA in the body, ARS results more efficient than DHA at inducing apoptosis in both TE671 and RD18 ERMS cells *in vitro*, suggesting that use of ARS instead of DHA could confer additional advantages against tumor growth *in vivo*.

Supplementary material

Supplementary Figures 1–6 can be found at http://carcin.oxfordjournals.org/

Funding

Associazione Italiana per la Ricerca sul Cancro (Project No. 6021); Ministero dell'Università e della Ricerca (PRIN-2012N8YJC3); Fondazione Cassa di Risparmio di Perugia (Project No. 2007.0218.020).

Acknowledgements

We wish to thank Pier-Luigi Lollini (Bologna, Italy) for providing RD18 cells.
Conflict of Interest Statement: None declared.

References

1. Parham, D.M. et al. (2006) Rhabdomyosarcomas in adults and children. An update. Arch. Pathol. Lab. Med., 130, 1454–1465.
2. Keller, C. et al. (2013) Mechanisms of impaired differentiation in rhabdomyosarcoma. FEBS J., 280, 4323–4334.
3. Parham, D.M. et al. (2013) Classification of rhabdomyosarcoma and its molecular basis. Adv. Anat. Pathol., 20, 387–397.
4. Tiffin, N. et al. (2003) PAX7 expression in embryonal rhabdomyosarcoma suggests an origin in muscle satellite cells. Br. J. Cancer, 89, 327–332.
5. Zammit, P.S. et al. (2006) Pax7 and myogenic progression in skeletal muscle satellite cells. J. Cell Sci., 119(Pt 9), 1824–1832.
6. Chiappalupi, S. et al. (2014) Defective RAGE activity in embryonal rhabdomyosarcoma cells results in high PAX7 levels that sustain migration and invasiveness. Carcinogenesis, 35, 2382–2392.
7. Charytonowicz, E. et al. (2009) Alveolar rhabdomyosarcoma: is the cell of origin a mesenchymal stem cell? Cancer Lett., 279, 126–136.
8. Rubin, B.P. et al. (2011) Evidence for an unanticipated relationship between undifferentiated pleomorphic sarcoma and embryonal rhabdomyosarcoma. Cancer Cell, 19, 177–191.
9. Wachtel, M. et al. (2010) Targets for cancer therapy in childhood sarcomas. Cancer Treat. Rev., 36, 318–327.
10. Eastman, R.T. et al. (2009) Artemisinin-based combination therapies: a vital tool in efforts to eliminate malaria. Nat. Rev. Microbiol., 7, 864–874.
11. Miller, L.H. et al. (2011) Artemisinin: discovery from the Chinese herbal garden. Cell, 146, 855–858.
12. Crespo-Ortiz, M.P. et al. (2012) Antitumor activity of artemisinin and its derivatives: from a well-known antimalarial agent to a potential anticancer drug. J. Biomed. Biotechnol., 2012, 247597.
13. Meshnick, S.R. (2002) Artemisinin: mechanisms of action, resistance and toxicity. Int. J. Parasitol., 32, 1655–1660.

14. Mercer, A.E. et al. (2011) The role of heme and the mitochondrion in the chemical and molecular mechanisms of mammalian cell death induced by the artemisinin antimalarials. J. Biol. Chem., 286, 987–996.
15. Lai, H.C. et al. (2013) Development of artemisinin compounds for cancer treatment. Invest. New Drugs, 31, 230–246.
16. Odaka, Y. et al. (2014) Dihydroartemisinin inhibits the mammalian target of rapamycin-mediated signaling pathways in tumor cells. Carcinogenesis, 35, 192–200.
17. World Health Organization. (2006) Guidelines for the Treatment of Malaria. WHO Press, Geneva, Switzerland.
18. Berger, T.G. et al. (2005) Artesunate in the treatment of metastatic uveal melanoma–first experiences. Oncol. Rep., 14, 1599–1603.
19. Lollini, P.L. et al. (1991) Reduced metastatic ability of *in vitro* differentiated human rhabdomyosarcoma cells. Invasion Metastasis, 11, 116–124.
20. Riccardi, C. et al. (2006) Analysis of apoptosis by propidium iodide staining and flow cytometry. Nat. Protoc., 1, 1458–1461.
21. Riuzzi, F. et al. (2007) RAGE expression in rhabdomyosarcoma cells results in myogenic differentiation and reduced proliferation, migration, invasiveness, and tumor growth. Am. J. Pathol., 171, 947–961.
22. Hou, J. et al. (2008) Experimental therapy of hepatoma with artemisinin and its derivatives: *in vitro* and *in vivo* activity, chemosensitization, and mechanisms of action. Clin. Cancer Res., 14, 5519–5530.
23. Rossetto, D. et al. (2012) Histone phosphorylation: a chromatin modification involved in diverse nuclear events. Epigenetics, 7, 1098–1108.
24. Lu, C. et al. (2008) Serum starvation induces H2AX phosphorylation to regulate apoptosis via p38 MAPK pathway. FEBS Lett., 582, 2703–2708.
25. Rao, P.K. et al. (2006) Myogenic factors that regulate expression of muscle-specific microRNAs. Proc. Natl. Acad. Sci. USA, 103, 8721–8726.
26. van Rooij, E. et al. (2008) MicroRNAs flex their muscles. Trends Genet., 24, 159–166.
27. Williams, A.H. et al. (2009) MicroRNA control of muscle development and disease. Curr. Opin. Cell Biol., 21, 461–469.
28. Feng, Y. et al. (2013) A feedback circuit between miR-133 and the ERK1/2 pathway involving an exquisite mechanism for regulating myoblast proliferation and differentiation. Cell Death Dis., 4, e934.
29. Novák, J. et al. (2013) MicroRNAs involved in skeletal muscle development and their roles in rhabdomyosarcoma pathogenesis. Pediatr. Blood Cancer, 60, 1739–1746.
30. Chen, J.F. et al. (2010) microRNA-1 and microRNA-206 regulate skeletal muscle satellite cell proliferation and differentiation by repressing Pax7. J. Cell Biol., 190, 867–879.
31. Olguin, H.C. et al. (2007) Reciprocal inhibition between Pax7 and muscle regulatory factors modulates myogenic cell fate determination. J. Cell Biol., 177, 769–779.
32. Riuzzi, F. et al. (2014) RAGE signaling deficiency in rhabdomyosarcoma cells causes upregulation of PAX7 and uncontrolled proliferation. J. Cell Sci., 127(Pt 8), 1699–1711.
33. Stevens, M.C. (2005) Treatment for childhood rhabdomyosarcoma: the cost of cure. Lancet. Oncol., 6, 77–84.
34. Galluzzi, L. et al. (2012) Molecular definitions of cell death subroutines: recommendations of the Nomenclature Committee on Cell Death 2012. Cell Death Differ., 19, 107–120.
35. Zhou, B.B. et al. (2000) The DNA damage response: putting checkpoints in perspective. Nature, 408, 433–439.
36. Falck, J. et al. (2002) The DNA damage-dependent intra-S phase checkpoint is regulated by parallel pathways. Nat. Genet., 30, 290–294.
37. Puri, P.L. et al. (2000) Induction of terminal differentiation by constitutive activation of p38 MAP kinase in human rhabdomyosarcoma cells. Genes Dev., 14, 574–584.
38. Yan, D. et al. (2009) MicroRNA-1/206 targets c-Met and inhibits rhabdomyosarcoma development. J. Biol. Chem., 284, 29596–29604.
39. Subramanian, S. et al. (2008) MicroRNA expression signature of human sarcomas. Oncogene, 27, 2015–2026.
40. Chen, J.F. et al. (2006) The role of microRNA-1 and microRNA-133 in skeletal muscle proliferation and differentiation. Nat. Genet., 38, 228–233.
41. Zhang, D. et al. (2012) Attenuation of p38-mediated miR-1/133 expression facilitates myoblast proliferation during the early stage of muscle regeneration. PLoS One, 7, e41478.
42. Rao, P.K. et al. (2010) Distinct roles for miR-1 and miR-133a in the proliferation and differentiation of rhabdomyosarcoma cells. FASEB J., 24, 3427–3437.
43. Tao, J. et al. (2012) microRNA-133 inhibits cell proliferation, migration and invasion in prostate cancer cells by targeting the epidermal growth factor receptor. Oncol. Rep., 27, 1967–1975.
44. Taulli, R. et al. (2009) The muscle-specific microRNA miR-206 blocks human rhabdomyosarcoma growth in xenotransplanted mice by promoting myogenic differentiation. J. Clin. Invest., 119, 2366–2378.
45. Kim, H.K. et al. (2006) Muscle-specific microRNA miR-206 promotes muscle differentiation. J. Cell Biol., 174, 677–687.
46. Breneman, J.C. et al. (2003) Prognostic factors and clinical outcomes in children and adolescents with metastatic rhabdomyosarcoma–a report from the Intergroup Rhabdomyosarcoma Study IV. J. Clin. Oncol., 21, 78–84.
47. Oberlin, O. et al. (2008) Prognostic factors in metastatic rhabdomyosarcomas: results of a pooled analysis from United States and European cooperative groups. J. Clin. Oncol., 26, 2384–2389.
48. Fernández-Briera, A. et al. (2010) Effect of human colorectal carcinogenesis on the neural cell adhesion molecule expression and polysialylation. Oncology, 78, 196–204.